Theoretical and Computational Acoustics
D. Lee, Y-H Pao, M.H. Schultz, and Y-C Teng (Editors)

3-D Irregular Grids' Optimization for the Tomographic Inversion of the Ocean Sound Speed

Gualtiero Boehm and Aldo Vesnaver
Osservatorio Geofisico Sperimentale, P.O. Box 2011, 34016 Trieste, Italy

Abstract

Irregular grids allow to fit the parameter number and distribution to the complexity of the sought velocity field and to the available data. It is so possible to reduce or eliminate the ambiguities due to the null space in the linearized traveltime inversion, introducing a priori information (where and if available) in the model space. We describe this method by a 3-D example for oceanographic studies, trying to detect a current tube in the layered sea water. We show the dependence of the image quality on the spatial distribution of sources and receivers and on the ray paths. The latter depend also on the wave types we consider, i.e. transmitted and reflected arrivals.

Introduction

The development of new technologies for reconstructing the structure of the ocean sound speed is rapidly growing. In their pioneering work, Munk and Wunsch (1979) used an immersed vertical array of receivers to detect the water layers in the surrounding area, recording the impulses emitted by a moving ship. Boehm et al. (1994, 1995) and Vesnaver (1995) showed that useful results may be achieved in 2-D by adopting the acquisition geometry that is typical of marine profiles for seismic exploration: a cable towed by

a ship in a horizontal position. This acquisition geometry is not optimal for oceanographic studies, because allows to detect a couple of water layers and to estimate the average vertical sound speed between the sea floor and surface. On the other hand, it exploits the information contained in the seismic profiles acquired worldwide with a small extra cost. In this paper we extend this analysis to 3-D, discussing different acquisition geometries with some vertical arrays of receivers. Considering a 3-D example, we reconstruct the spatial inhomogeneities due to a current tube in the surrounding layered sea water. We show that the images of the water structure can be improved by fitting iteratively irregular grids to the velocity field estimated in sequence. We show also that it is possible to reduce the number of receiver arrays (and so the costs) if we jointly invert the reflected and transmitted signals.

Regular or irregular grids ?

In the linearized inversion, the traveltimes of acoustic signals are related to the unknown slowness field (inverse of velocity) by a set of linear equations. In the tomographic approach, the unknowns are the slowness values in the pixels, which are small homogeneous domains usually regularly shaped as squares or rectangles. A basic drawback of this approach is that a null space exists, making the inversion solution non-unique. This happens because the linear system is often underdetermined and, also when apparently overdetermined, it may be rank deficient. In this way, the velocity estimates obtained are often unstable and (at least) unreliable. We do not need irregular grids to transform an underdetermined problem into an (apparently) overdetermined one: it is sufficient to reduce the pixel number by increasing the spatial sample interval of the regular grid. So we pay the stability increase by a resolution loss; but irregular grids are important, if we like to squeeze out of our data as much information as possible. Reducing too much the global resolution of the grid, we may loose some interesting local detail in the tomographic image. The causes of the rank deficiency of the tomographic matrix are linearly dependent equations (i.e. ray paths) and uncrossed pixels. We can easily remove the second one by merging adjacent pixels, but is less obvious what we should do to transform the ray paths into independent. Vesnaver (1994) showed that we can move and split the pixel boundaries by analysing the local energy of the null space. His method relies

on the singular value decomposition of the tomographic matrix (that is a global estimate), which allows to measure the local reliability of the velocity value in each pixel. Where this measure is low or zero, we should merge adjacent pixels into one, while the domains covered by various independent rays can be split into smaller pixels. In this paper we follow a more intuitive approach, assuming that a priori information is available. As a first step, we invert the traveltimes by a conventional regular grid, such that the pixel number is comparable with that of the available rays. By interpreting the image obtained, we try to identify some nearly homogeneous zones: here, we merge pixel groups into one; viceversa, we can split them into finer others in the areas where we see or expect some velocity anomaly.

3-D example

Figure 1 displays a 3-D model composed by 9 water layers, with a thickness of 100 metres each and a sound speed comprised between 1508 and 1516 m/s. The total depth is so 0.9 km, while the length and width are 3 and 1 km respectively. A straight current tube, with an oblique direction with respect to the model limits, causes a velocity anomaly, with values ranging from 1518 to 1522 m/s. The model simulates a real condition commonly found in the Eastern Mediterranean Sea (i.e. the Levantine intermediate water). We remark that the velocity anomaly is a small fraction (less than 0.4This fact produces two opposite effects. First, we can neglect the ray bending due to the Snell's law: this makes the problem really linear and simplifies our calculations. On the other hand, we cannot expect a clear evidence of the anomaly: the traveltime differences with respect to the unperturbed medium could be too small with respect to the available precision in the data and in the software implementation. Figure 2 shows the acquisition geometry we considered first. We put a set of 10 vertical arrays at the left side of the model, each composed by 8 receivers, and the same number and distribution of sources at the opposite side. We connected each source with each receiver by a ray associated to the transmitted wave, and computed the corresponding 6400 traveltimes. We considered initially a regular model, composed by 9 layers as the true model. Each layer was subdivided into a grid of 5x15 pixels, so that the total pixel number is 675. The inversion methods we used are the ART and SIRT algorithms (van der Sluis and van der Vorst,

1987). The initial velocity value guessed in all pixels is 1500 m/s. During the inversion we used global constraints, forcing everywhere the estimated values to be comprised between 1500 and 1530 m/s. The traveltime inversion (Figure 3) revealed a velocity increase both in the central part (due to the current tube) and in the central layer (due to the surrounding water structure). Nevertheless, the image is quite blurred, and we cannot distinguish the boundaries of the current tube. Looking at this first image, we cannot claim that the water layers around the anomaly are homogeneous; on the other hand, we can decide to concentrate our attention to the central part, neglecting possible minor oscillations elsewhere. So we modified the grid by merging the pixels of the first, second, eighth and ninth layer into one for each layer. Furthermore, we doubled their number in the central part, where a 10x15 grid was set at each layer. In the image so obtained (Figure 4), the velocity anomaly is better resolved. We concentrated then our attention to the fifth layer, leaving the 10x15 grid, but reducing the resolution in the third, fourth, sixth and seventh layers, where a 4x8 sampling was used. The resolution of the tube current is so further improved (Figure 5), because now we can probably suppose that its direction is oblique with respect to the model. The acquisition geometry we used till now (Figure 2) may be too expensive for real experiments, and so we considered a second pattern (Figure 6). Here we simulated only four vertical arrays (with 8 receivers each) and 5 lines of 15 sources at the surface. The latter ones could be easily provided by a ship with a single source travelling along those lines. As before, we traced rays from each source to each receiver, but for both transmitted and reflected signals. Their total number is 4800, which is comparable to that of the previous acquisition geometry. We assume that the depth and shape of the reflecting sea floor is known. This is a strong but not unrealistic hypothesis. If the sea floor is not known from independent information, we can exploit the reflected arrival themselves to get a quite accurate estimate of its depth. For the description of methods to recover it, we send the reader to Dyer and Worthington (1988) and Carrion et al. (1993 a, b), which present also applications to marine seismic data. Figure 7 shows the image provided by an ART reconstruction using the same regular grid as in Figure 3. We can notice various instabilities everywhere. The fourth layer displays correctly a higher velocity with respect to the others, but we cannot recognize there any local anomaly. Therefore, we tested the SIRT algorithm with the same data and grid, since it provides generally smoother and more robust

results (at the price of a slower convergence). The better image obtained (Figure 8) suggested us to verify the superiority of the SIRT for the previous acquisition geometry, and we got indeed a smoother image also in that case (Figure 9). We remark that in other cases of interest for hydrocarbons exploration, where the velocity contrasts are much larger, the ART methods performs quite often better than SIRT. So we would suggest to adopt ART or SIRT methods where the expected velocity changes are, respectively, sharp or smooth. These experiences encouraged us to use the SIRT approach in our further tests. Adopting the same irregular grids as in the Figures 4 and 5 but with the new acquisition geometry, we improved the corresponding images in the same way (Figures 10 and 11, respectively). In the second acquisition geometry, the contributions of transmitted and reflected waves are complementary. Inverting separately the transmitted (Figure 12) or reflected arrivals (Figure 13), we get a worse result in both cases. In particular, using only the transmitted waves the image is blurred in the deeper zone, where the ray coverage is poorer; viceversa, reflected arrivals reconstruct better the lower part of the tube current.

Conclusions

Irregular grids allow to optimise the local resolution with respect to the available data and to the (initially unknown) velocity field. They are an implicit way to introduce a priori information, because they limit (or allow) the velocity changes in the model space. Focusing our attention at the desired target, we can reduce the parameters to be estimated (and the computational cost), stabilising the inversion procedure and increasing the solution reliability. We considered two different acquisition geometries in a 3-D example, and showed that the joint inversion of reflected and transmitted waves let to simplify the data acquisition, with a probable cost reduction. This is due not only to the double number of rays exploited, but to the different paths of the two wave types, which allow a much better coverage of the tomographic grid. The second geometry of sources and receivers considered here is not only cheaper in terms of acquisition costs, but provides also better resolved images, despite the smaller number of picked traveltimes. This experience confirms that the rays' number is less important than their spatial relationship with the tomographic grid.

Acknowledgement

This work was partially supported by the European Community in the Joule II Programme (contract n. JOU2-CT93-0321).

References

Boehm G., Crise A. and Vesnaver A. 1994. Pycnocline identification applying travel time tomography to marine seismic data. Proceedings of the 2nd European Conference on Underwater Acoustics, L. Bjoernoe (ed.), European Commission, 1075-1080.

Boehm, G., Crise, A. and Vesnaver, A. 1995. Travel time inversion of marine seismic data for ocean sound speed reconstruction. In: 'Full field inversion methods in ocean and seismo-acoustics', O. Diachok et al. (eds), Kluwer, 291-296.

Carrion, P., Boehm, G., Marchetti, A., Pettenati, F., and Vesnaver, A. 1993 a. Reconstruction of lateral gradients from reflection tomography. J. Seis. Expl., 2, 55-67.

Carrion, P., Marchetti, A., Boehm, G., Pettenati, F., and Vesnaver, A. 1993 b. Tomographic processing of Antarctica's data. First Break, 11, 295-301.

Dyer, B. C. and Worthington, M. H. 1988. Seismic reflection tomography: a case study: First Break, 6, 354-366.

Munk W. and. Wunsch C. 1979. Ocean acoustic tomography: A scheme for large scale monitoring. Deep-Sea Research 26A, 123-161.

van der Sluis, A., and van der Vorst, H. A. 1987. Numerical solution of large, sparse linear algebraic systems arising from tomographic problems, in Nolet, G., Ed., Seismic tomography with applications in global seismology and exploration geophysics: D. Reidel Publ. Co.

Vesnaver A. 1994. Towards the uniqueness of tomographic inversion solutions. Journal of Seismic Exploration 3, 323-334.

Vesnaver, A. 1995. Null space reduction in the linearized tomographic inversion. In: 'Full field inversion methods in ocean and seismo-acoustics', O. Diachok et al. (eds), Kluwer, 139-145.

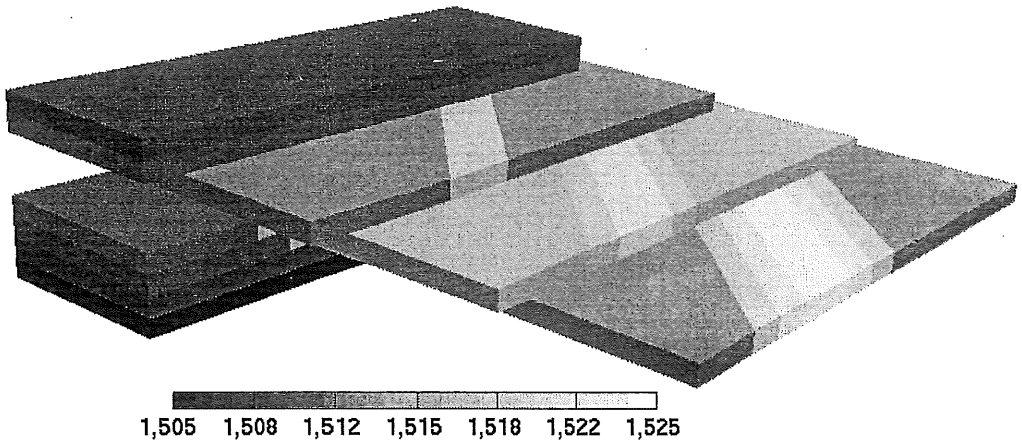

Figure 1 – Synthetic 3–D model simulating a current tube in the intermediate Levantine water, that is typical of the Eastern Mediterranean Sea.

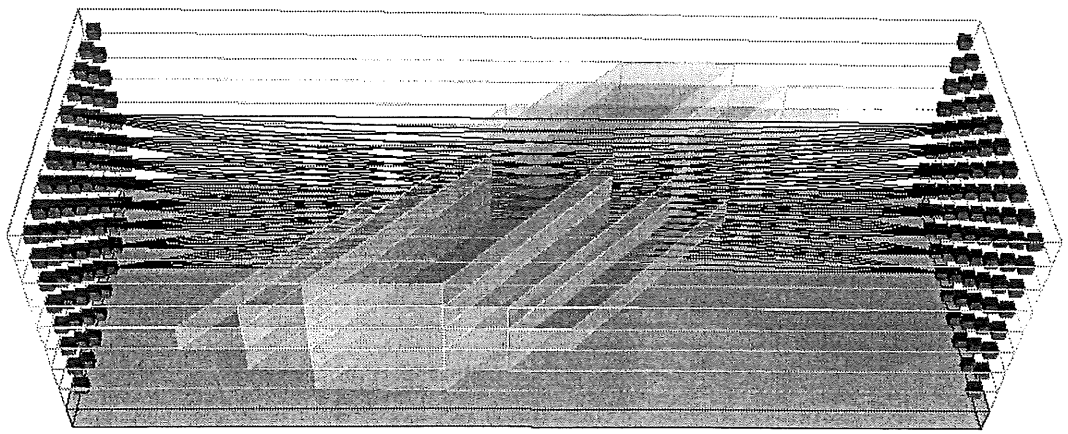

Figure 2 – Acquisition geometry 1: the little cubes correspond to the simulated sources and recivers. Some rays in a plane are drawn crossing the current tube.

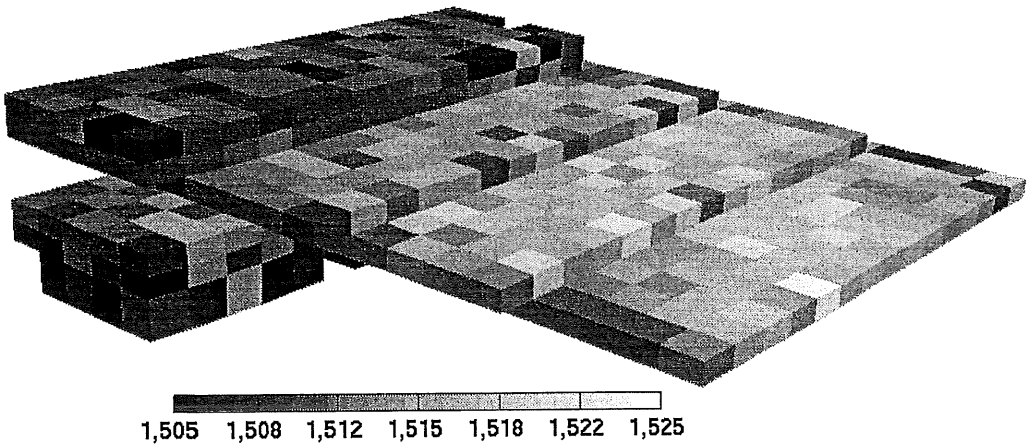

Figure 3 — Tomographic inversion of transmitted arrivals using the ART method in a regular grid (geometry 1). The pixels not drawn correspond to velocity out of the grey tone scale.

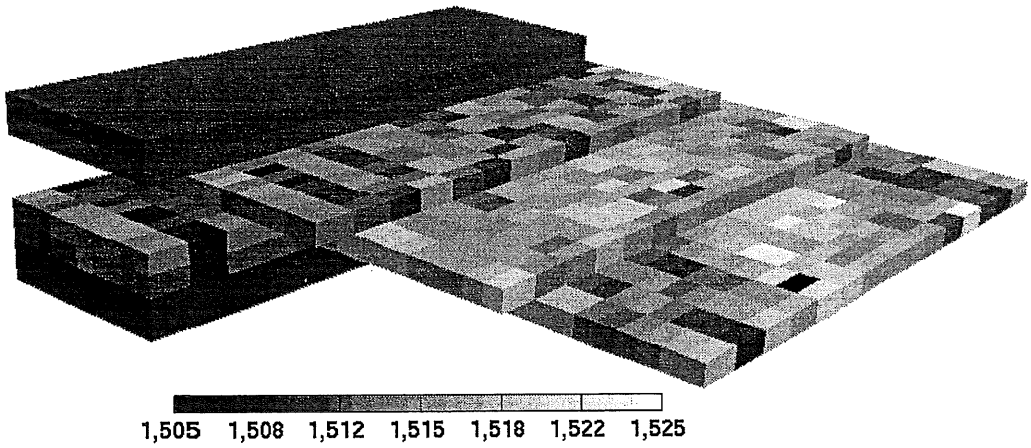

Figure 4 — Tomographic inversion of transmitted arrivals using the ART method in the first irregular grid (geometry 1).

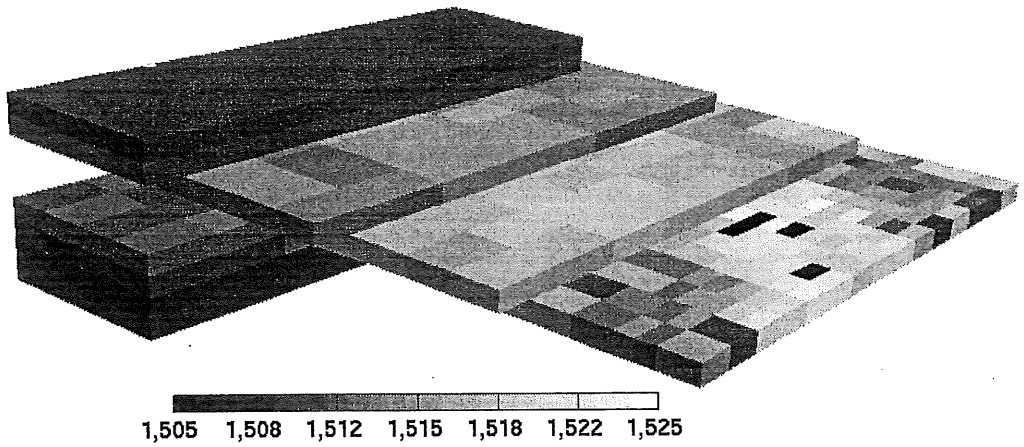

Figure 5 – Tomographic inversion of transmitted arrivals using the ART method in the second irregular grid (geometry 1).

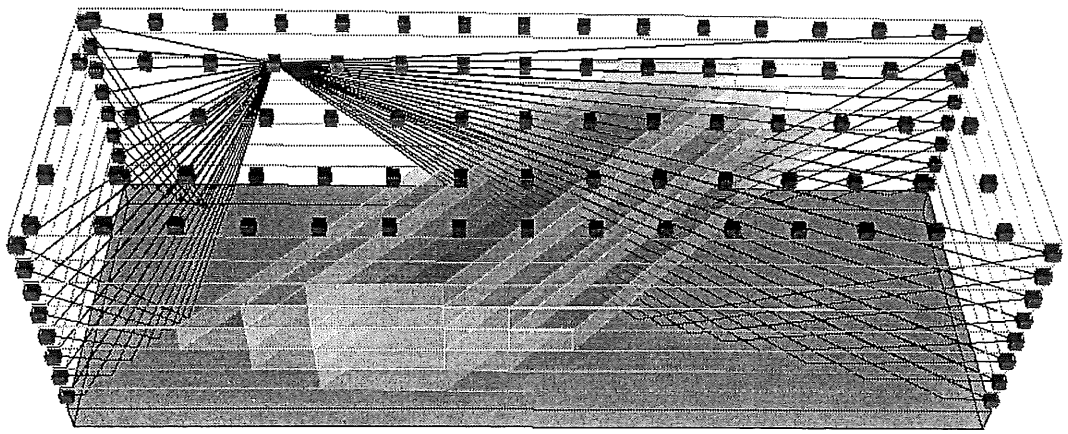

Figure 6 – Acquisition geometry 2: the little cubes correspond to the simulated sources and recivers. Some rays of reflected and transmitted waves from a source at the surface are drawn.

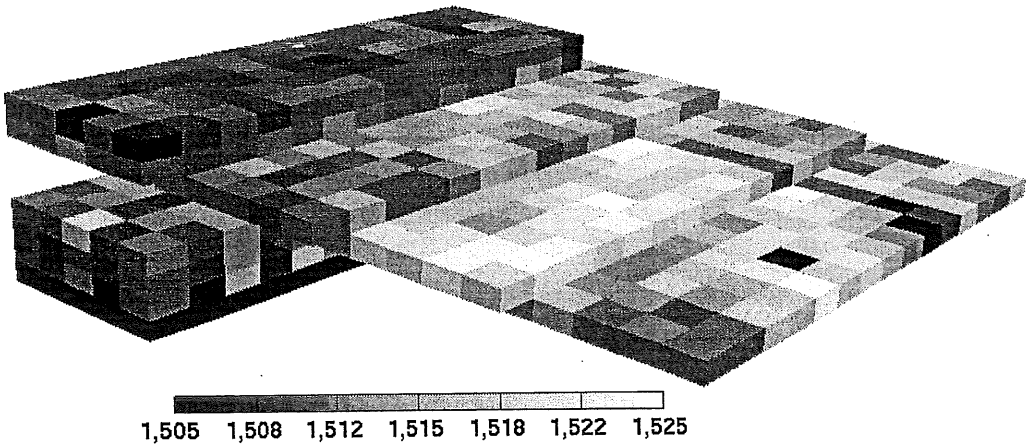

Figure 7 – Tomographic inversion of transmitted and reflected arrivals, using the ART method in a regular grid (geometry 2).

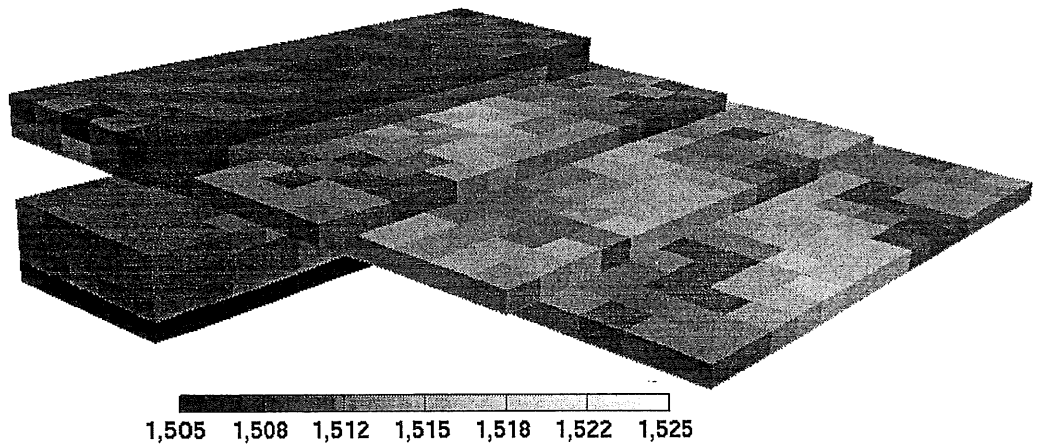

Figure 8 – Tomographic inversion of transmitted and reflected arrivals, using the SIRT method in a regular grid (geometry 2).

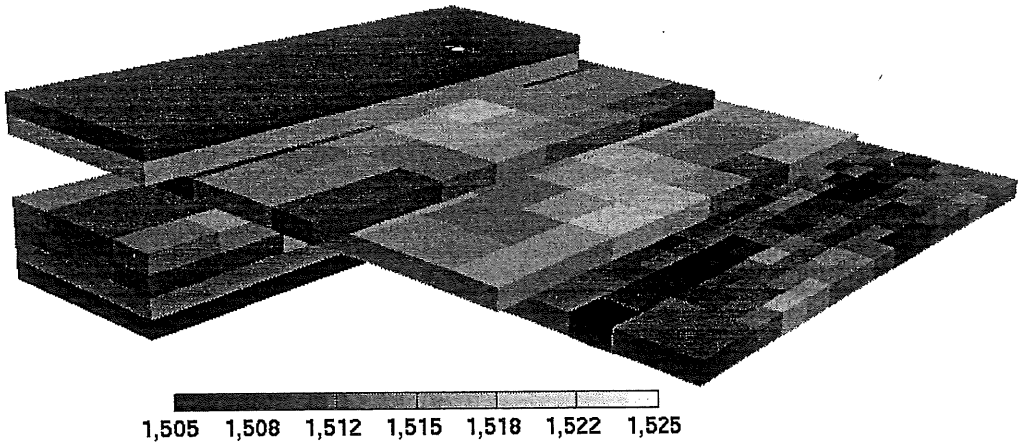

Figure 11 – Tomographic inversion of transmitted and reflected arrivals, using the SIRT method in the second irregular grid (geometry 2).

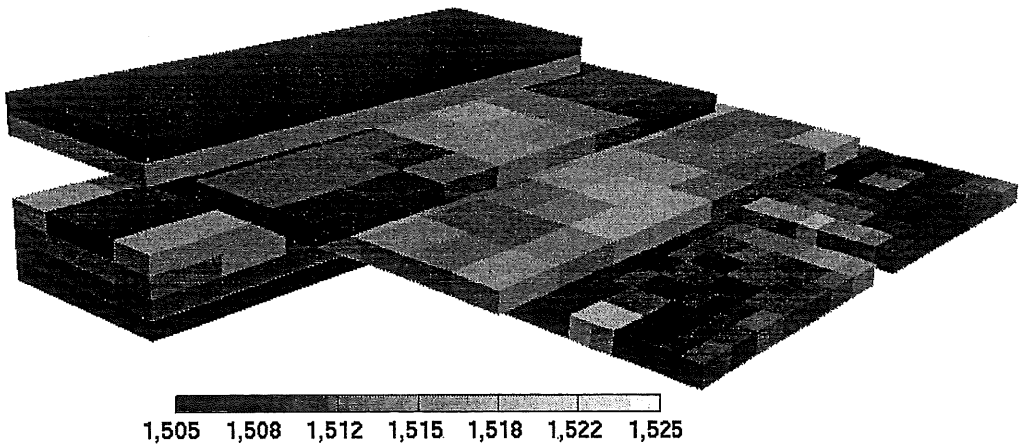

Figure 12 – Tomographic inversion of transmitted arrivals only, using the SIRT method in the second irregular grid (geometry 2).

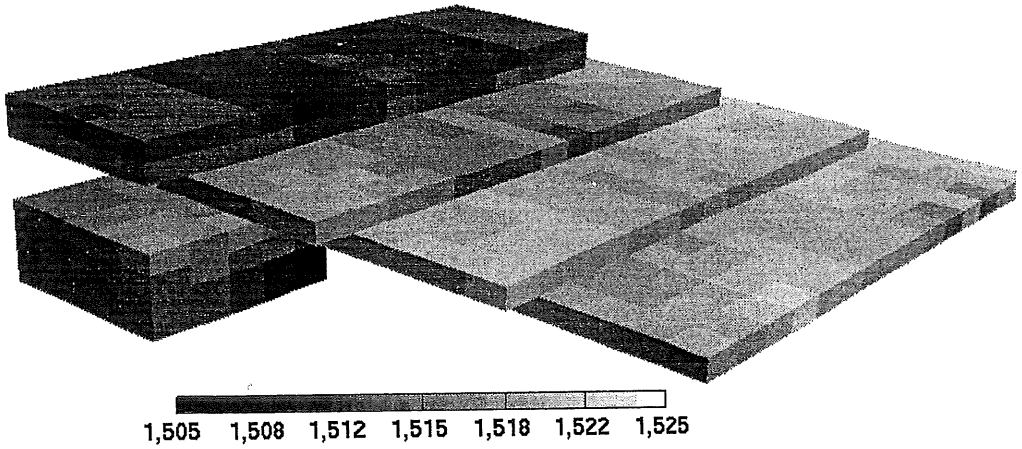

Figure 9 – Tomographic inversion of transmitted arrivals only, using the SIRT method in a regular grid (geometry 1).

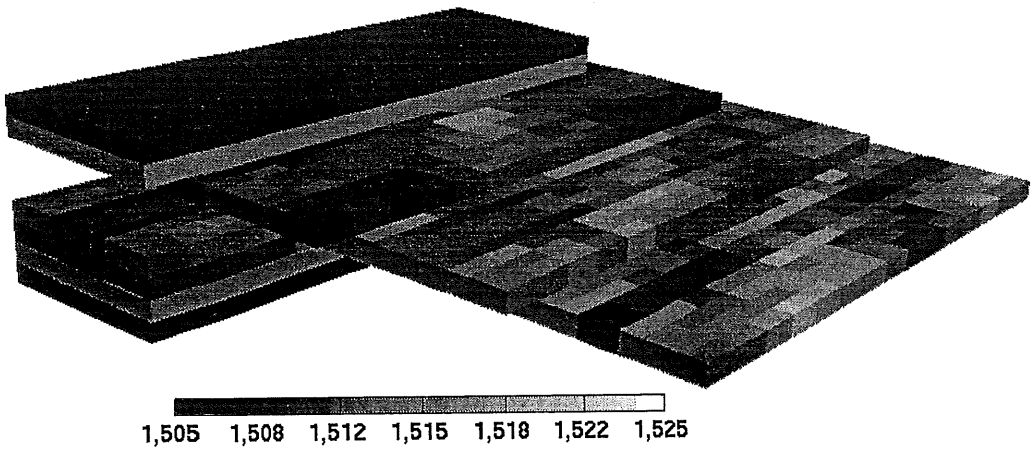

Figure 10 – Tomographic inversion of transmitted and reflected arrivals, using the SIRT method in the first irregular grid (geometry 2).

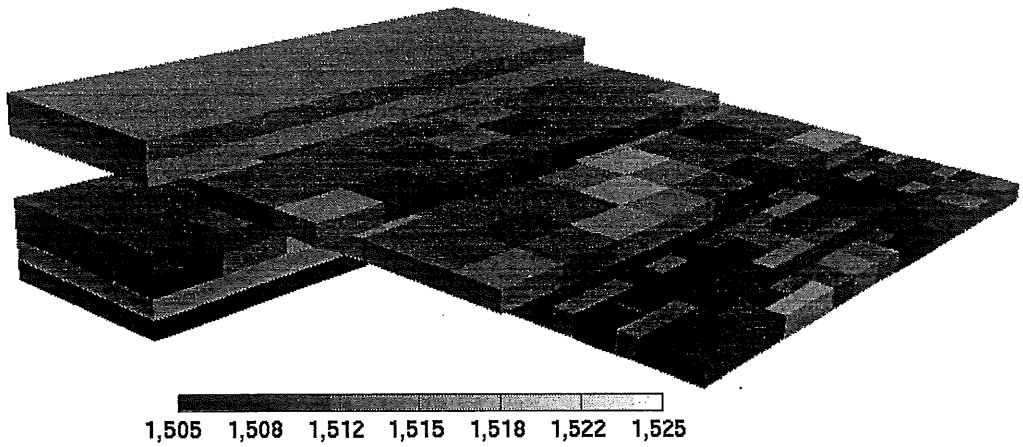

Figure 13 – Tomographic inversion of reflected arrivals only, using the SIRT method in the second irregular grid (geometry 2).